DYNAMIC CRACK PROPAGATION AND CRACK ARREST BEHAVIOUR OF TWO LOW ALLOY STEELS.

E Bouyne*, T Iung+ and A. Pineau*.

A technique developed recently in our Institute to investigate crack initiation, rapid crack propagation and crack arrest with a single specimen was applied to two low alloy steels (16MND5 and 15CD910) with a tempered bainitic microstructure. This technique is based on tests on cracked ring specimens submitted to a compressive load applied to the poles of the ring while a crack is located in the equatorial plane at the outer surface of the specimen. The main interest of this geometry lies in the variation of the stress intensity factor, K with crack length which follows a bell-shaped curve. The experiments were carried out at -196°C. This condition produced brittle cleavage fracture. It is shown that the fracture toughness at crack arrest, K_{1a}, may largely be lower than the fracture toughness at crack initiation, K_{1c}. Moreover K_{1a} is a decreasing function of the crack velocity.

INTRODUCTION

The fracture toughness at crack arrest, K_{1a}, could become a parameter for designing structures such as nuclear reactors. The standardized way to measure K_{1a} is referenced in [1]. The technique involves CCA specimens which leads to a decreasing stress intensity factor, K_I with crack length. A number of authors have shown the importance of dynamic effects such as wave reflections at the free surfaces of the specimens. Moreover boundary conditions are not easily controlled during the test. A novel technique was developed recently [2, 3] to investigate crack initiation, rapid crack propagation and crack arrest with a single specimen. This technique is based on tests on cracked ring specimens submitted to a compressive load applied to the poles of the ring while a crack is located in the equatorial plane at the outer surface of the specimen. There are two advantages in comparison with other specimens : the boundary conditions are well controlled and the round shape of the specimen reduces waves reflection effects from free

* Centre des Matériaux - Ecole des Mines de Paris, BP87 91003 Evry (France), URA CNRS 866
+Now with IRSID, Physical Metallurgy Department, Voie Romaine, BP 320, 57214 Maizières lès Metz (France).

boundary surfaces allowing us to use a static analysis to investigate crack arrest [2].

This test was applied to two low alloy steels : 16MND5 [4] and 15CD910. Tests were carried out at -196°C to produce cleavage fracture.

After a brief description of the materials and experimental procedures, we will present the experimental results, especially those concerning crack arrest, and the results of microscopical observations.

MATERIALS AND EXPERIMENTAL PROCEDURES

▫ *Materials*

The materials investigated are two low-alloy steels. 16MND5 steel (ASTM designation A508 class 3) is used in nuclear power stations to manufacture the pressure vessels. 15CD910 steel is used for the manufacture of thermal power stations components. The compositions of these steels are shown in **Table 1**. These materials were submitted to an oil quench heat-treatment which provided a bainitic microstructure. The yield strength for 16MND5 steel is 686 MPa at 20 °C and 1150 MPa at -196 °C while it is 542 MPa and 1144 MPa at the same temperatures for 15CD910 steel. The fracture toughness at -196°C is approximately 40 MPa$\sqrt{m}$ for 16MND5 steel [4] and 30 MPa$\sqrt{m}$ for 15CD910 steel.

	C	Mn	Ni	Cr	Mo	S	P
16MND5	0.16	1.30	0.77	0.22	0.49	0.0018	0.008
15CD910	0.14	0.54	0.07	2.25	1.01	0.003	0.004

Table 1 : Chemical composition in weight percent.

▫ *Experimental procedures*

Fig 1 shows a sketch of the ring test specimen. The ring is defined by its external and internal radii, R_2 and R_1. A radial crack, of length a, is located in the equatorial plane. The geometry is characterized by two dimensionless parameters : $\beta = R_1/R_2$ and $\lambda = a/(R_2-R_1)$. The dimensions of the ring are initially R_1 = 32.5 mm and R_2 = 75 mm. The thickness B is 20 mm. The specimen is precracked from a starter notch, by fatigue compressive loading at room temperature. The ring is then machined to achieve its final dimensions : R_2 = 65 mm, β = 1/2 and B = 12 mm.

The ring is submitted to a compressive load P_0. **Fig 1** shows the zones where local stresses are tensile and compressive with respect to the y axis. If the load is sufficient a crack can initiate and stop when approaching the compressive zone. A finite element calculation gives the variation of K_I versus crack length. This variation can be written as:

$$K_1 = \frac{P_0}{B\sqrt{R_2}} k(\lambda) \qquad (1)$$

where k is an adimensional parameter which is a function of λ for a given value of β, as shown in **Fig 2**. Eq. (1) is the result of a static analysis. Iung [2] showed that such an analysis is sufficient. After the test, the measurement of initial crack length, final crack length and the use of the bell-shaped curve allow us to evaluate the fracture toughness at initiation K_{1C} and the fracture toughness at arrest K_{1A} (the load P_0 remains almost constant during crack propagation).

A gauge is glued on the surface of the specimen. It is made of a number of wires which produce a voltage step ($\approx$ 0.5 V) when they break. The location and the distance (1.27 mm) between two wires being known, we can follow the evolution of the crack tip position and measure the crack speed. A high speed memory oscilloscope, triggered by the breaking of the first wire, records the signal. **Fig 3** shows an example of one of these recordings.

A clip gauge extensometer measures the crack mouth opening and is used to detect the instant of fracture and the corresponding load P_0.

The test is carried out in liquid nitrogen (θ = -196 °C) to ensure brittle fracture.

Some observations were made by scanning electron microscopy on fracture surfaces and on longitudinal sections of 15CD910 cracked specimens. Further results on 16MND5 material are given elsewhere [4].

EXPERIMENTAL RESULTS

▫ *Crack speed*

Fig 3 shows an example of an oscilloscope recording which can be used to determine the crack speed. We can observe that the crack tip has a period of acceleration and a period of deceleration until it stops. The maximum crack speed seems to occur where the crack tip is most loaded (see **Fig 2**, the maximum of k; k_m). The accuracy of such a recording is not sufficient to be more precise. Similar observations were reported by Küppers [5] on glass.

For each test we can determine a maximum crack speed (see **Fig 3**). This parameter will be used to analyse the fracture toughness at crack arrest. Maximum crack speeds reached with our two steels were included between 100 m/s and 800 m/s. High crack speeds can easily be obtained with small initial crack lengths.

▫ *Fracture toughness at arrest*

We have plotted the results of K_{1a} measurements in **Fig 4**. In both materials it is observed that the fracture toughness at crack arrest is a decreasing function of crack speed, which suggests that K_{1a} is not an intrinsic material characteristic. At low crack velocities, K_{1a} values are similar to those of K_{1c}. At large crack speeds (V_{max} > 500 m/s), the K_{1a} values can reach values as small as about 5 MPa$\sqrt{m}$.

Moreover a large scatter in the results is observed since, for the same crack speed, K_{Ia} values can differ by a factor of almost 2. Similar behaviour was noticed recently in a low alloy pipe-line steel [2, 3]. Our observations are also in agreement with those made by a number of authors (see, eg [6]) who showed that the values of K_{Ia} were a decreasing function of crack jumps in CCA type specimens. In those specimens the crack speed is likely to be an increasing function of crack jump.

▫ ***Microstructural observations.***

After being tested, the specimens are submitted to a blue tinting heat treatment. This allows us to distinguish clearly the fracture surface, the initial and final crack front. **Fig 5a** shows a photograph of a 15CD910 specimen. Most of the fracture surface is covered by cleavage facets. Nevertheless we can see all along the crack path some areas that appear in white on S.E.M photographs (**Fig 5a**). These areas are parts of the material that broke by ductile tearing, as proved by the presence of dimples on the ligaments. All these ductile ligaments are elongated in the direction of propagation, and their thickness is about 10 μm. Some of the ligaments near the crack arrest front appear bright which means that they were unbroken before final opening.

Fig 5b shows a longitudinal section of a 15CD910 cracked specimen before final opening. This photograph shows that the crack is quite discontinuous and that some regions remain unbroken behind the crack front. These ligaments are more numerous when we approach the crack arrest front. This indicates that the opening of the crack involves the deformation and the fracture of the ligaments by either cleavage or ductile tearing (see **Fig 5a**). In this micrograph a number of microcracks along the crack path can be observed. Progressive sectioning of the specimen was used to investigate the three-dimensional aspect of the arrested cracks. These observations showed that the microcracks observed in Fig 5b were interconnected and formed a continuous network surrounding islands of unbroken material.

These observations are similar to those of Hoagland et al. [6] made on other materials (4340 steel, A-517 steel, Mild steel and Fe-3Si steel). Moreover they confirm the ideas of Dvorak [7]. According to this author, some parts of the material "favourably oriented" can cleave easily ("easy cleavage") forming a continuous three-dimensional network and leaving unbroken ligaments behind the crack tip. The ligaments need to deform plastically before breaking. Hoagland et al. [6] have shown in a Fe-3Si material that plastic deformation was confined in these ligaments.

CONCLUSIONS

Two bainitic steels were tested to measure crack arrest fracture toughness at -196°C with a ring shape specimen. In both cases it is concluded that K_{Ia} is a

decreasing function of the maximum crack speed. Therefore K_{Ia} cannot be considered as an intrinsic material parameter.

Fractographic observations showed the existence of unbroken ligaments left behind the front of the arrested crack and the complex 3D aspect of the fracture surfaces.

REFERENCES

[1] ASTM E1221, Annual Book of ASTM Standards, 1988.
[2] T. Iung and A. Pineau to appear in *Fatigue Fract. Engng. Mater. Struct.*
[3] T. Iung and A. Pineau to appear in *Fatigue Fract. Engng. Mater. Struct.*
[4] H. Jaeckel, T. Iung and A. Pineau, *Fatigue Fract. Engng. Mater. Struct.*, Vol. 17, 1994, pp. 1281-1293.
[5] H. Kuppër, *Int. J. Fract. Mech.*, Vol 3, 1967, pp. 13-17.
[6] R. G. Hoagland, A. R. Rosenfield and G. T. Hahn, *Metallurgical Transactions*, Volume 3, January 1972, pp. 123-136.
[7] J. Dvorak, *Fracture*, Ed. by Pratt, Chapman, 1969, pp. 338-349.

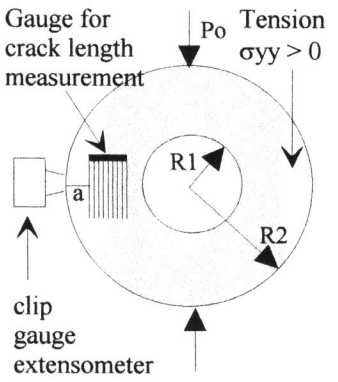

Fig 1 : Sketch of the ring test specimens. The locations where the stresses are tensile are shown.

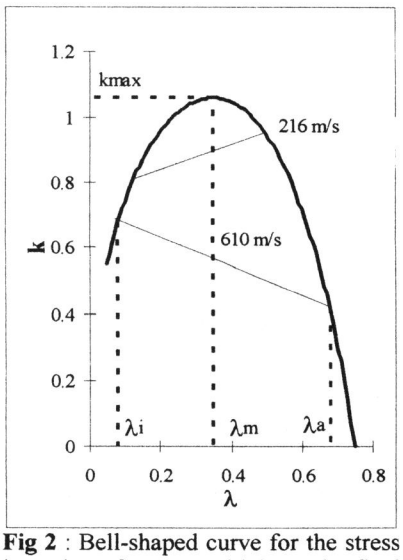

Fig 2 : Bell-shaped curve for the stress intensity factor. Initial and final positions of two cracks are given.

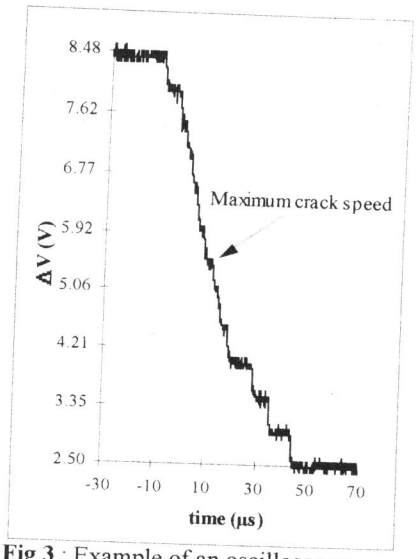

Fig 3 : Example of an oscilloscope recording for crack speed measurement

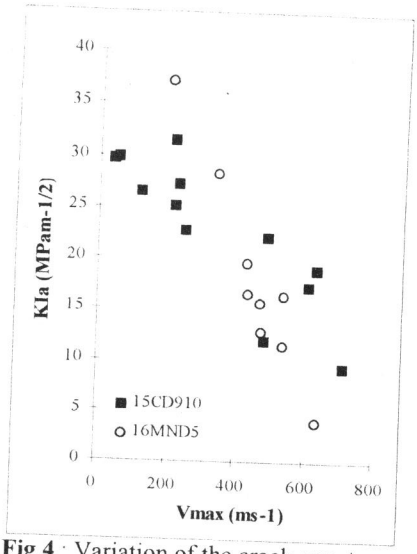

Fig 4 : Variation of the crack arrest fracture toughness with maximum crack velocity.

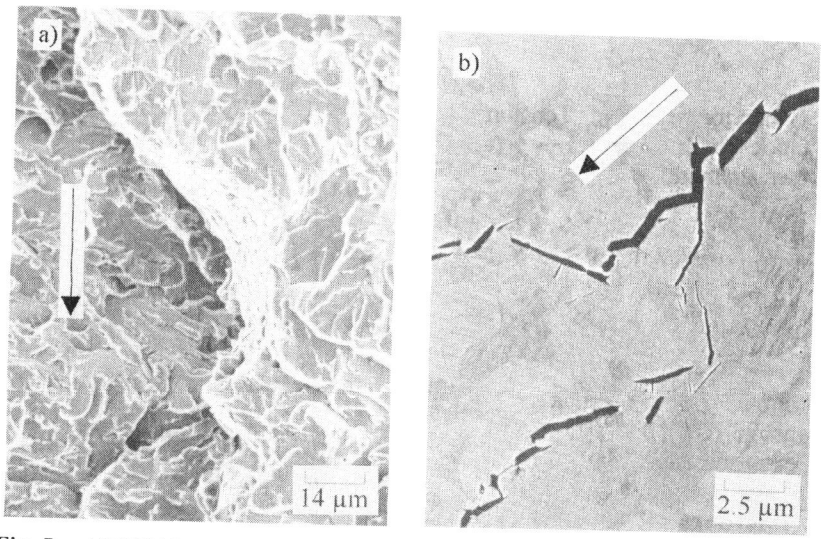

Fig 5 : 15CD910 material. **a)** Fracture surface showing ductile ligament, **b)** longitudinal section. The propagation direction of the main crack is indicated by an arrow.